IEEE Access
Multidisciplinary | Rapid Review | Open Access Journal

SPECIAL SECTION ON WIDE AREA SURVEILLANCE

Received July 30, 2019, accepted August 16, 2019, date of publication August 28, 2019, date of current version September 23, 2019.

Digital Object Identifier 10.1109/ACCESS.2019.2938011

Massively Parallel Implementation of FETI-2LM Methods for the Simulation of the Sparse Receiving Array Evolution of the GRAVES Radar System for Space Surveillance and Tracking

ANTOINE JOUADÉ AND ANDRÉ BARKA
ONERA/DEMR, Université de Toulouse, 31055 Toulouse, France

Corresponding authors: Antoine Jouadé (antoine.jouade@onera.fr) and André Barka (andre.barka@onera.fr)

This work was supported in part by the French Defense Procurement Agency [Direction Générale de l'Armement (DGA)] through the contract for the GRAVES refurbishment and upgrades with a partial EU SST Program, and in part by the Grand Equipement National de Calcul Intensif (GENCI) Grant c2014109083.

ABSTRACT This paper presents the massively parallel implementation of the FETI-2LM techniques (Finite Element Tearing and Interconnecting with two Lagrange Multipliers) in the FACTOPO code to solve large-scale sparse receiving array evolutions of the GRAVES bistatic radar in the VHF band. There are four main ingredients in the proposed work and methodology: 1) the implementation of a total field weak formulation of FETI-2LM algorithms for multi-sources modeling using an efficient block Krylov recycling strategy for the calculation of the hundreds of antenna embedded radiation patterns of the sparse array; 2) the implementation of a meshing strategy consisting in generating the sparse array by populating a regular periodic grid; 3) the implementation of the proposed methodology on massively parallel clusters; 4) the investigation of performances of the optimized GRAVES elementary antenna in the VHF band, followed by the demonstration of the expected gain performances even with stronger interferences due to the densification of the array. These simulations of the GRAVES sparse array requiring the resolution of sparse linear systems with 10.47 billion unknowns have been made possible thanks to recent developments of the FETI-2LM domain decomposition method and the use of 13, 692 Intel Xeon Broadwell E5-2680v4 computing cores. A total of 3.8 million cumulated hours have been invested in the interest of the augmentation of the antennas. Until now FETI-2LM methods have been successfully implemented for antenna and diffraction electromagnetic simulations in the S-C-X-Ku and Ka bands and to the best to our knowledge this is the first time that they have been used in the VHF band.

INDEX TERMS Aerospace control, bi-static radar, Doppler radar, digital beamforming, low earth orbit satellites, parallel machines, supercomputers, radar tracking, real-time systems, space surveillance and tracking, sparse array, very-high frequencies, wide area surveillance, finite element methods, finite element tearing and interconnecting, FETI, domain decomposition methods, VHF band, FACTOPO.

I. INTRODUCTION

The GRAVES System (*Grand Réseau Adapté à la VEille Spatiale* = Large Radar Array for Space Surveillance) [1] is a Space Surveillance and Tracking (SST) system [2]–[4], whose main mission is to construct a space picture for military intelligence by autonomously building and maintaining a catalog of space objects. GRAVES is owned by the French Ministry for the Armed Forces, and is operated by the French Air and Space Force. Its performances have enabled over 300 objects in Low Earth Orbit (LEO) to be detected and catalogued. The GRAVES system is a bistatic radar

The associate editor coordinating the review of this article and approving it for publication was Mehmet Alper Uslu.

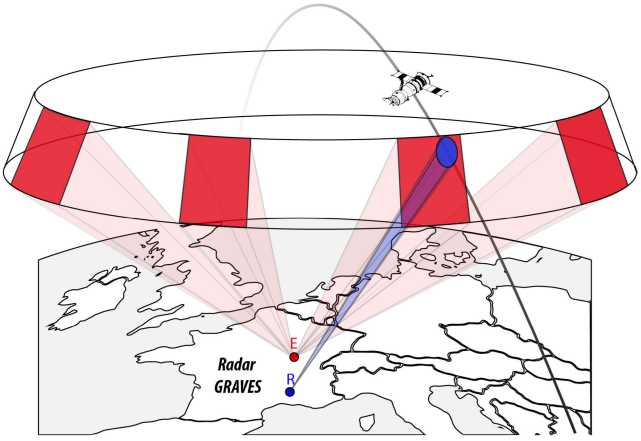

FIGURE 1. Illustration of the principle of the GRAVES bistatic radar with E: Emitter and R: Receiver.

(see Figure 1) working with a VHF continuous wave pure carrier transmission at 143.05 MHz. The transmission site corresponds to four linearly polarized transmitting arrays, each covering 45° in azimuth and 30° in elevation. Each Field-of-View (FoV) is individually scanned by electronic deflection forming a fence in the sky. A coverage of 180° in azimuth allows the detection of each satellite at least once every 24 hours. The reception site, shown in Figure2, 400 km south of the transmission site (to ensure a good decoupling and to avoid saturating the reception stages), is a 60 m diameter sparse array of circularly-polarized antenna elements [1] that receives the signals reflected by the Low Earth orbiting objects crossing the FoV. Circular polarization allows arbitrary linearly-polarized signals influenced by the ionosphere due to the Faraday effect to be received.

The digital beamforming (DBF) performed at the reception level enables the localization of the objects along the azimuth and the elevation, while the frequency shift caused by the Doppler effect enables the radial velocity, and hence the orbit altitude, to be determined. There are few equivalents to the GRAVES radar strictly designed for space surveillance, and we can cite the following works and achievements described in References [5]–[7]. Other functional equivalents of large surveillance radars designed for advanced alert are American [8] or Russian [9]; they contribute to space surveillance but are not sized to this mission. There are no functional equivalents in Europe; GRAVES is the only way system able to do so, leading France to be among the only 4 nations with this ability to monitor and autonomously build a catalog of space objects. GRAVES is a unique and original concept, which is its strength. ONERA, associated with the SME Degréane Horizon, has been notified by the DGA, the French Defense Procurement Agency, for the refurbishment contract aimed at extending the life time of the system up to 2030, while improving the overall performance in order to detect smaller objects (cubsat satellites and space debris) over great distances. The lifetime extension involves updating the transmission and reception systems as well as the processing chain. The performance enhancements that are of interest in this article are the receiving antenna element performance improvement and the densification of the receiving array by

FIGURE 2. Photography of the sparse receiving array.

investigating, through full-wave electromagnetic simulation, the coupling effects of a more populated sparse array on the overall array performance. These investigations would have a positive impact on the overall link budget, enabling new objects to be detected and catalogued. The foreseen evolutions would make GRAVES an even more valuable key contributor to the SST segment.

In the field of electromagnetic simulation, it is now well established that the Finite Element Method (FEM) is one of the most successful frequency domain computational methods [10]. The method is now intensely implemented by engineers and designers often interested in full-wave computation of complete systems, and of their possible environments [10]–[12]. These methods are now widely spread through commercial software such as CST Microwave Studio [13] and HFSS [14]. Such simulations can be very complex, especially when the problems of interest involve multi-scale geometries with very fine features. The FEM combines, very efficiently, a geometrical adaptability and ability to handle arbitrary materials for modeling complex geometries and materials of arbitrary composition, including meta-materials currently intensely used in modern antennas. Finite element approximation of Maxwell's equations leads to a sparse linear system, usually solved by using direct or iterative solvers. However, modern engineering applications dealing with antennas, scatterers or microwave circuits, require the solution of problems with billions of unknowns. In order to efficiently simulate complex electromagnetic problems of large size compared to the wavelength, multidomain and multimethod coupling schemes based on generalized scattering matrix computations of 3-D sub-domains have been developed [15] and implemented for antenna siting [12], [16], [17] as well as diffraction problems [18]. The global target is split into sub-domains separated by fictitious surfaces. For each sub-domain (even the exterior 3-D volume), the Generalized Scattering Matrix (GSM) is computed with different methods such as the FEM, the Electric Field Integral Equation (EFIE) or the Combined Field Integral Equation (CFIE) combined with a generalized field expansion on the fictitious surfaces with spectral basis functions [17] or modal basis functions [15]. Then, the different objects are connected together by cascading the various matrices. Within a context of parametric investigations, the scattering matrices of the modified domains have to be re-evaluated, the others are simply re-used in the connection step. This strategy significantly reduces the computation time compared to traditional hybrid methods for which a geometric or electromagnetic modification requires a new computation of the complete target. Furthermore, the matrix computations are totally independent, allowing code and data protection within the context of industrial consortium projects. This GSM-based strategy has been enriched with asymptotic Physical Optics (PO) techniques [19] but is, however, quite difficult to implement for the GRAVES reception array and was not retained.

We preferred to implement some recent advances in Domain Decomposition Methods (DDM), especially the Finite Element Tearing and Interconnecting with two Lagrange multipliers (FETI-2LM) technique, to solve large-scale FEM problems with multiple right-hand sides encountered in electromagnetic applications (up to several hundreds of embedded antennas in the GRAVES project). DDMs were initially developed for the efficient parallel solution of elliptic problems and are based on consistent enforcement of the Dirichlet boundary conditions at the interface, by using the Schur complement method [20], or by using Neumann boundary conditions at the interface, as in the FETI method [21]. The FETI method was extended to the solution of Helmholtz equations using Robin interface boundary conditions, which led to the FETI-H method [22], and which is based on the early work of [23]. For the Helmholtz equations, the FETI-H method has been efficiently improved for multiple right-hand sides with recycling Krylov methods [24], [25]. FETI methods have been successfully extended to the solution of Maxwell equations (FETI-2LM) in the frequency domain for the calculation of antenna arrays and metamaterial periodic structures [26], [27] and equipped with recycling Krylov methods [28], [29] to speed-up multi-source applications.

The first particularity of this work is the implementation of Krylov type iterative algorithms (recently proposed in [30]), in order to improve the FETI-2LM domain decomposition method to solve multi-source electromagnetic problems. This is very attractive in the GRAVES context, where we have to calculate the embedded radiation patterns of hundreds of antennas before performing the digital beamforming (DBF) at the reception level. The principle is to store all search direction vectors for the condensed interface problems arising from the successive sources (elementary antennas) and to use them to build a projection that decreases the number of iterations for the successive sequences of Krylov iterations. The first algorithm is based on a projection technique and the second combines the projection technique with a block strategy consisting in simultaneously computing several blocks of search directions for several right-hand sides. It has been shown in [30], through the solution of two engineering applications, that both methods can greatly reduce the number of iterations for convergence by increasing the memory used for recycling the Krylov vectors. For scattering applications and plane wave illuminations, it has been observed that the projection strategy allows a drastic reduction of the number of iterations from the second incidence. The block strategy not only reduces the number of iterations for the successive sources, but also enhances the parallel efficiency of the FETI-2LM method. This feature is particularly beneficial for the computation of the radiation efficiency of an antenna array (scattering parameters and embedded radiation patterns). Indeed, unlike plane wave excitation, the local antenna feed with TEM ports provides very different near field solutions from one port to another. It has been shown in [30], on antenna arrays that the computation for few linearly independent right-hand sides with the block strategy offers a speed increase of 11.17. This FETI-2LM method

implemented in ONERA's FACTOPO code has also been recently optimized for the simulation of non-periodic and multi-scale transmit-arrays [31], and is therefore naturally preferred for the simulation of the hundreds of antennas populating the GRAVES receiving sparse array.

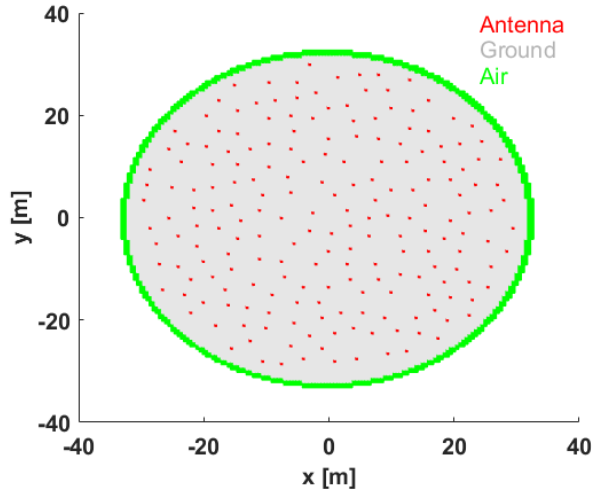

FIGURE 3. Subdomain decomposition of the densified GRAVE sparse receiving array.

The second particularity of our implementation of the Finite Element Tearing and Interconnecting method is the fact that the complete mesh is not built upstream of the resolution of the electromagnetic problem and, consequently, a specific mesh splitter tool such as METIS [32] is not necessary to decompose the large-scale initial mesh (60 m diameter disk) into sub-domains, as was done, for example, for array antennas covered by a radome in [33]. Our method is general, based on parallel-thinking, and tailored to efficiently introduce 3D non-periodic grids with sub-domains that are not necessarily of the same size (VHF antenna, ground plane cells and empty sub-domains described in Figure 3). Each sub-domain in our decomposition is equipped with its own local mesh, belonging to a limited set of unit-cell meshes, generated separately with an automatic procedure of the GID preprocessor [34]. Thus, the geometry of very complex sparse array antennas is represented efficiently with only a few local meshes (three for GRAVES arrays). Furthermore, since the method is implemented on parallel machines, each compute core with at least 4 GB of memory is allocated exclusively to a sub-domain (elementary cell of the sparse array). One can easily implement relatively fine meshes in each sub-domain, rendering the sometimes very slow adaptive mesh refinement techniques unnecessary.

The third particularity of this work is the simulation on massively parallel clusters using MPI programming of two GRAVES sparse arrays: the initial configuration and the densified configuration. This kind of resources available at ONERA is not farfetched, and is required for the demonstration of the gain efficiency of the densified configurations despite the coupling and shadowing effects due to the VHF antennas.

The paper is organized as follows. Section II briefly recalls the FETI-2LM formulation, proposes further developments to take into account, through a total field formulation, a waveguide mode excitation feeding the antenna with block Krylov multi-source algorithms to speed-up the GRAVES embedded antenna diagram simulations. In Section III a method is proposed and its accuracy for the discretization of the sparse array with three types of sub-domains (VHF antenna, empty and ground plane) is discussed. In Section IV, a recent optimization of the unit-cell antenna is proposed followed in Section V by the demonstration of gain performances obtained after densification of the sparse receiving array.

II. FETI-2LM FORMULATION (THEORICAL REMINDERS)

The FETI-2LM method proposed to solve the Maxwell equations [26], [27], [35], is based on the decomposition of the global computational domain in non-overlapping sub-domains (Figure 4), in which local solution fields are calculated by solving the finite-element system with a direct method. Tangent field continuity is then imposed at the interfaces by using 2 Lagrange multipliers, which leads to a reduced problem at the interfaces that can be solved using an iterative method. The solution of the interface problem is then used as a boundary condition to evaluate the fields in each sub-domain.

The Ampère-Maxwell Law and Faraday's Law can be combined to yield a single-order vector wave equation.

We denote by $\Omega = \Omega_1 \cup \Omega_2 \cup \ldots \cup \Omega_N$ a partition of the initial computation domain (Figure 4). In each sub-domain Ω_i, the total electric and magnetic fields $\mathbf{E^i}$, $\mathbf{H^i}$ satisfies:

$$\nabla \times (\mu_{r,i}^{-1} \nabla \times \mathbf{E^i}) - k_0^2 \epsilon_{r,i} \mathbf{E^i} = 0 \tag{1}$$

Vectors $\mathbf{E^i_{incident}}$ and $\mathbf{H^i_{incident}}$ stand for the modal incident electric and magnetic field defined at the waveguide surface Γ_{port} of a unit normal n_{port} pointing inwards to volume Ω_i containing the modal source:

$$\mathbf{n_{port}} \times \mathbf{H^i} = \mathbf{n_{port}} \times \mathbf{H^i_{incident}} \tag{2}$$

$k_0 = \omega\sqrt{\epsilon_0 \mu_0}$ is the free-space wave number, $\epsilon_{r,i}$ is the relative permittivity in Ω_i and $\mu_{r,i}$ the relative permittivity in Ω_i. Γ_{ABC} represents the boundary of the volume Ω and n_{ext} represents its exterior normal, along which the scattered field satisfies absorbing boundary conditions (ABC):

$$\mathbf{n_{ext}} \times \nabla \times \mathbf{E^i_s} + jk_0 \mathbf{n_{ext}} \times (\mathbf{n_{ext}} \times \mathbf{E^i_s}) = 0 \tag{3}$$

On perfectly electric conducting surfaces Γ_{PEC}, the total electric field verifies the usual Perfectly Electric Conductor (PEC) boundary conditions:

$$\mathbf{n_{ext}} \times \mathbf{E^i} = 0 \tag{4}$$

In the following, $\mathbf{E^i_j}$ is the electric field on the interface of the sub-domain Ω_i adjacent to the sub-domain Ω_j (Figure 4). At interfaces Γ_{ij}^{robin} separating two sub-domains Ω_i and Ω_j, Robin type boundary conditions are imposed,

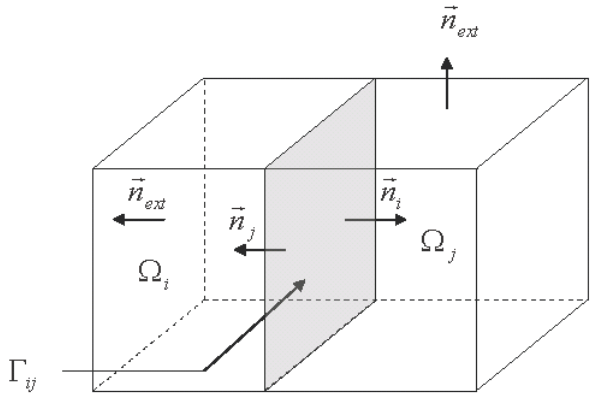

FIGURE 4. Interface problem [26].

by using Lagrange multipliers $\Lambda_{\mathbf{i}}^{\mathbf{j}}$ and $\Lambda_{\mathbf{j}}^{\mathbf{i}}$, which are the new unknowns:

$$\mathbf{n_i} \times (\mu_{r,i}^{-1} \nabla \times \mathbf{E_j^i}) + jk_0 \mathbf{n_i} \times (\mathbf{n_i} \times \mathbf{E_j^i}) = \Lambda_{\mathbf{j}}^{\mathbf{i}} \quad (5)$$

$$\mathbf{n_j} \times (\mu_{r,j}^{-1} \nabla \times \mathbf{E_i^j}) + jk_0 \mathbf{n_j} \times (\mathbf{n_j} \times \mathbf{E_i^j}) = \Lambda_{\mathbf{i}}^{\mathbf{j}} \quad (6)$$

Let us consider the following functional space:

$$H(curl, \Omega_i) = \{u \in L^2(\Omega_i)^3, \nabla \times u \in L^2(\Omega_i)^3\}.$$

The weak formulation used for the computation of the total field $\mathbf{E^i}$ belonging to space $H(curl, \Omega_i)$ in domain Ω_i and satisfying the PEC boundary condition (4) is obtained via the Galerkin method, which tests the wave equation (1) with the zero order Nedelec edge functions W ([36]).

$$\begin{aligned}\int_{\Omega_i} \left[\mu_{r,i}^{-1}(\nabla \times \mathbf{E^i}) \cdot (\nabla \times \mathbf{W}) - k_0^2 \epsilon_{r,i} \mathbf{E^i} \cdot \mathbf{W}\right] \mathrm{d}\Omega \\ + jk_0 \int_{\Gamma_{ext}} (\mathbf{n_{ext}} \times \mathbf{E^i}) \cdot (\mathbf{n} \times \mathbf{W}) \, \mathrm{d}\Gamma \\ + jk_0 \int_{\Gamma_{ij}^{robin}} (\mathbf{n_i} \times \mathbf{E_j^i}) \cdot (\mathbf{n} \times \mathbf{W}) \, \mathrm{d}\Gamma \\ = jk_0 \, Z_0 \int_{\Gamma_{port}} (\mathbf{n_{port}} \times \mathbf{H_{incident}^i}) \cdot (\mathbf{W}) \, \mathrm{d}\Gamma \quad (7)\end{aligned}$$

The iterative solution of the interface problem is based on the ORTHODIR Krylov sub-space method [37]. The problem to be solved thus becomes:

$$\Lambda_{\mathbf{j}}^{\mathbf{i}} + \Lambda_{\mathbf{i}}^{\mathbf{j}} - (M_j^i + M_i^j)\mathbf{E_i^j} = 0 \quad \forall i = 1, ..N \quad (8)$$

where j is neighboring i, and

$$M_j^i = jk_0 \int_{\Gamma_{ij}^{robin}} (\mathbf{n_i} \times \mathbf{W_i}).(\mathbf{n_i} \times \mathbf{W_i}) d\Gamma_{ij} \quad (9)$$

The iterative methods consists of four steps:

1) Compute local solutions in each sub-domain with the use of Robin type conditions by solving the problem (5,6).
2) Exchange fields $\mathbf{E_i^j}$ and Lagrange multipliers $\Lambda_{\mathbf{i}}^{\mathbf{j}}$ at each interface
3) Compute $\mathbf{g_j^i} = \Lambda_{\mathbf{j}}^{\mathbf{i}} + \Lambda_{\mathbf{i}}^{\mathbf{j}} - (M_j^i + M_i^j)\mathbf{E_i^j}$
4) Implement ORTHODIR with a stopping criterion $\|g\| < \varepsilon$

Once the problem has been solved for the first right hand-side (first antenna of the GRAVES sparse array) and a set of search direction vectors has been built, and if the Krylov space method is the ORTHODIR method, both these vectors and their products by the FETI operator have been computed and can be stored in memory. They provide a natural set of vectors to be used to implement a preconditioner based on projection for the next antenna. Thus, the initial set of vectors can be augmented, for each new right-hand side, with the set of newly computed search direction vectors. With this technique, the number of actual new iterations required for each new antenna tends to decrease dramatically. The previous recycling technique is very efficient for linearly-dependent right-hand sides (plane-wave excitations for example) which is not the case for linearly independent right-hand sides (translation of the antenna on the sparse array). A significant improvement of the previous Krylov recycling strategy called block Krylov recycling, whose main consequence is to improve the parallel efficiency of the method, is then implemented in the total field formulation for GRAVES simulations. It consists in solving the successive problems not one by one, but rather by blocks of a few (typically 10-20 antennas) at the same time. This technique consists in computing several search directions at each iteration of the interface problem and all of the search directions of the block are used for all of the antennas.

III. DOMAIN DECOMPOSITION STRATEGY USED FOR THE DISCRETIZATION OF THE SPARSE RECEIVING ARRAY

As indicated previously, the complete mesh of the dense sparse array (Figure 2), which is very tricky to achieve and requires considerable memory resources, is therefore not built in our simulation methodology. However, the FETI method in the frequency domain requires a mesh of each subdomain (each elementary antenna). The sparse array being incomplete and non-periodic, this pre-treatment step would be long and difficult to implement even with an automatic mesh splitter such as METIS. The strategy we propose in this work is to "populate" a regular grid of regular periodicity (less than the inter-element distance) with three types of sub-domains ("antenna", "ground plane" and "empty"). This strategy makes it possible to virtually build the mesh of the complete sparse array with only 3 sub-domain meshes ("antenna", "ground plane" and "empty"). These generic sub-domains will then be duplicated and translated to generate the complete sparse array. It was decided to use sub-domains of size x = 50 cm, y = 50 cm and z = 2.5 m. The size of 50 cm corresponds to a limit related to the size of the antenna element (48 cm diameter).

In Figure 3, we can observe the position and nature of the 13, 692 sub-domains that will be used in the simulation of the complete sparse array. As an example for a simulation with 200 antennas, the number of each type of sub-domains is:

- 200 "antenna" sub-domains

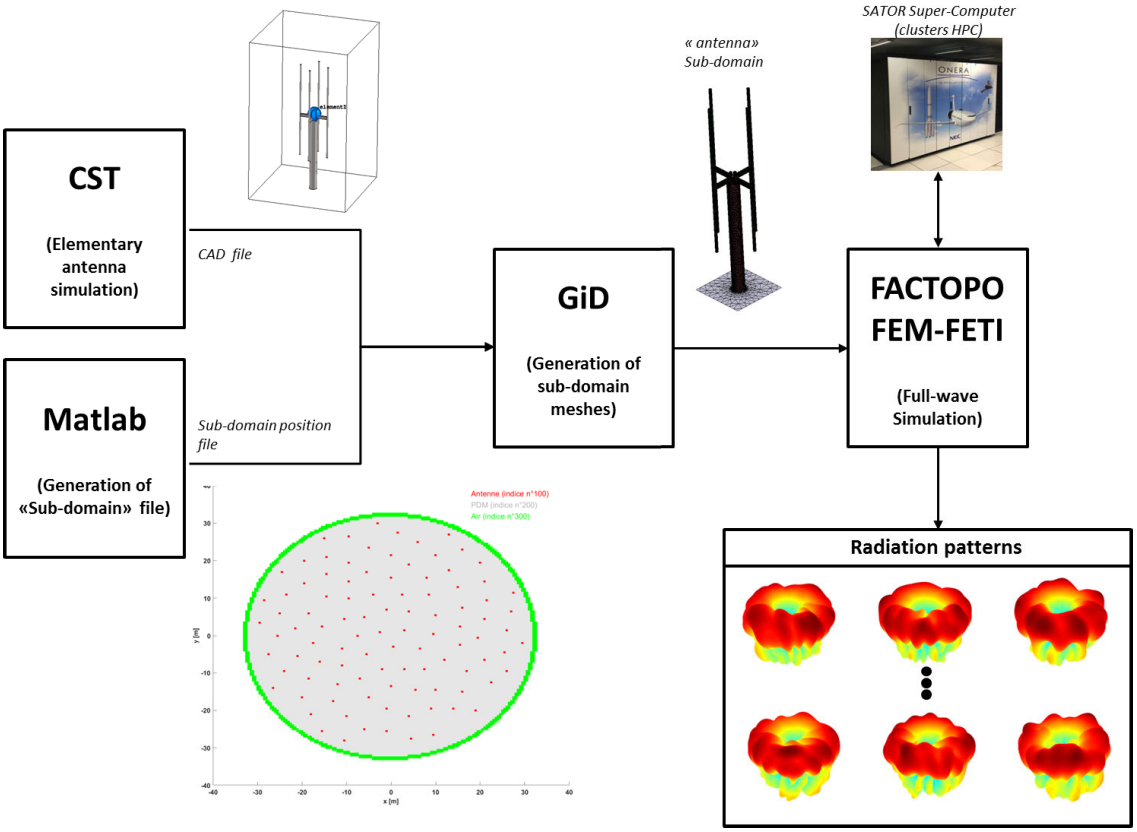

FIGURE 5. Simulation strategy of the GRAVES sparse array.

- 12, 592 "ground plane" sub-domains
- 800 "empty" sub-domains

Finally, in Figure 5, the simulation strategy used is shown:

- Step 1: Optimization of the unit-cell antenna with CST Microwave Studio [13] and generation of the 3D CAD files
- Step 2: Specification of the position of each sub-domain in the regular grid
- Step 3: From the 3D CAD files, mesh generation of the three sub-domains using the GiD preprocessor [34]
- Step 4: Factopo FEM-FETI simulations using ONERA's massively parallel SATOR cluster
- Step 5: Extraction of the radiation patterns of each embedded antenna element

IV. RECEIVING ANTENNA ELEMENT OPTIMIZATION

The element to be optimized is a circularly-polarized crossed-dipole antenna as shown in Figure 6, which consists of a set of two dipoles aligned at right angles to each other, with currents of equal magnitude that are in phase quadrature.

The two dipole antennas are fed by two separate ports with the requisite 90° phase difference between them thanks to a 3 dB 90° hybrid coupler. The coaxial tubes that feed the dipole antennas are surrounded by a sleeve balun with a depth of a quarter-wavelength. The element is placed on a flat electric conductor reflector. The presence of the surface redirects half of the radiation towards the opposite direction.

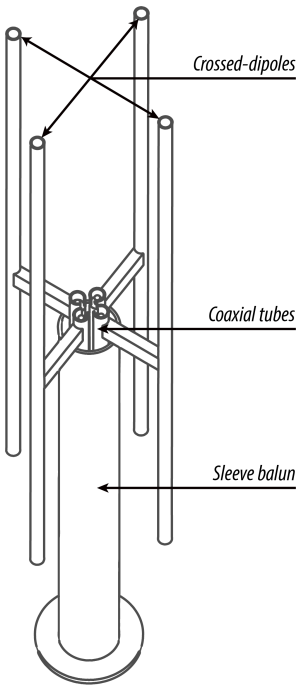

FIGURE 6. Sketch of the receiving antenna element.

The optimization goal is to improve the gain for arbitrary linear polarizations. In order to maximize the gain in all of the components, an antenna with optimized circular polarization

is required. This optimization should respect the following requirements:

- Isotropic radiation pattern along the azimuth with ripple lower than 1 dB
- Axial ratio of less than 1 dB
- Directive radiation pattern along the elevation with a half-power beamwidth of 30° from 45° to 75° in elevation, optimized with respect to the useful directions for beamforming

The optimization is performed on the lengths of both the horizontal and vertical arms of the dipoles and the height of the dipoles from the reflector.

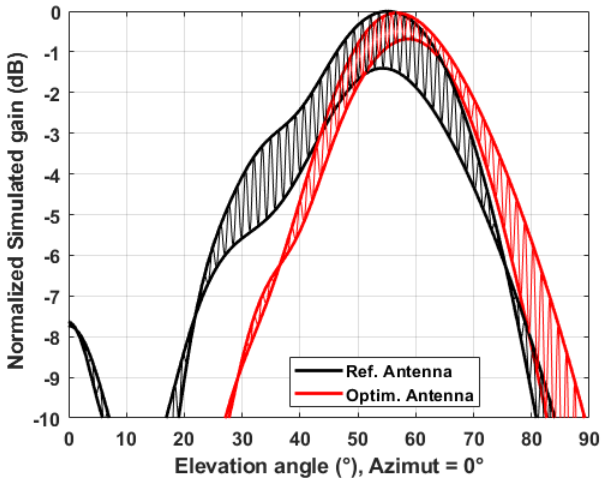

(a)

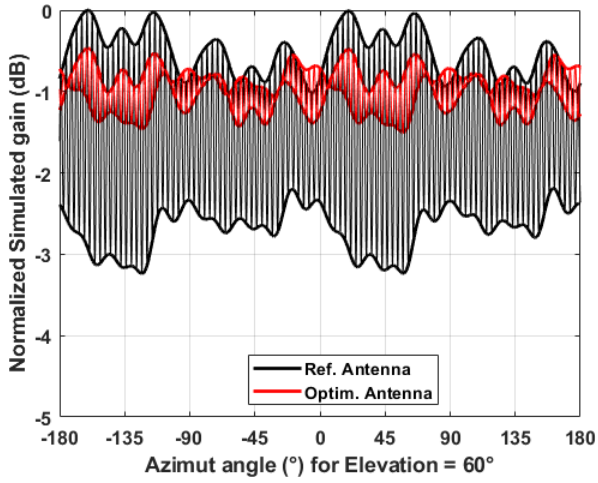

(b)

FIGURE 7. Normalized (maximum gain of reference antenna) radiation pattern in rotating linear polarization of the Reference antenna and the optimized antenna along (a) the azimuth axis and (b) the elevation axis.

Figure 7 shows a comparison of the radiation patterns of the reference antenna and the optimized antenna along both the elevation and the azimuth axis. In this figure, rotating linear polarization is used, meaning that the lower and the upper envelopes correspond to the minor and major axis of the

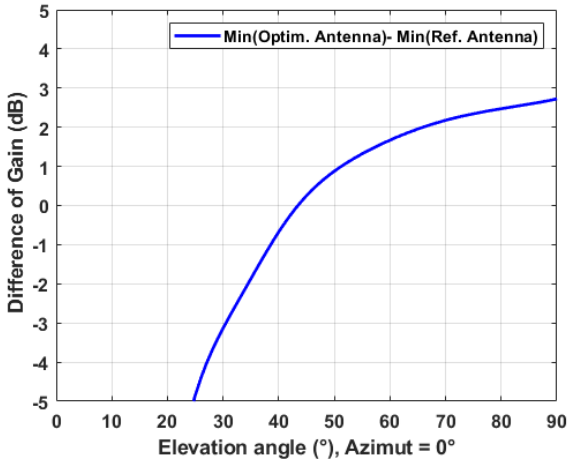

FIGURE 8. Difference in gain between the lower envelope of the optimized antenna and the lower envelope of the reference antenna.

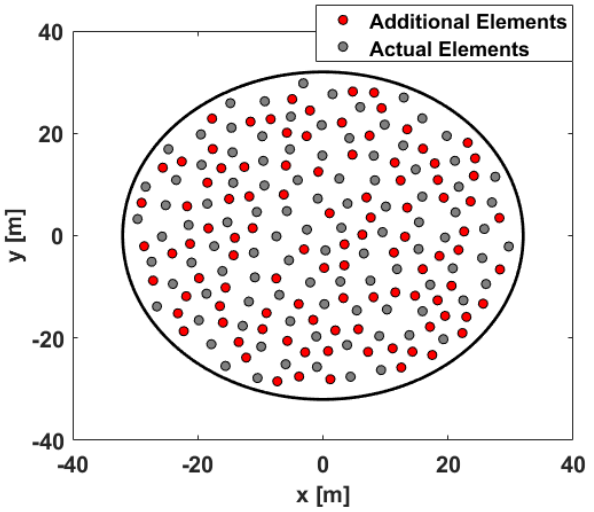

FIGURE 9. Array geometry with the actual antenna elements and with the additional elements.

elliptic polarization. The gain improvement has to be guaranteed for arbitrary linear polarization, hence a comparison of the lower envelopes of both the reference and the optimized antennas is shown in Figure 8.

Figure 7b shows that the optimized antenna has ripples of less than 0.8 dB along the azimuth axis at an elevation angle of 60°. Figure 7a shows that the difference of gain between the lower and upper envelopes of the optimized antenna is less than 1 dB between 45° and 75° which attests to a significant enhancement of the circular polarization. An improvement greater than 1 dB for arbitrary linear polarization is achieved for elevation angle between 52° and 90°.

V. EVALUATION OF THE DENSIFICATION OF THE RECEIVING ARRAY

Figure 9 shows both the actual and densified sparse array configurations. Examples of sparse array usage are available in the literature [38]. The GRAVES array has been determined

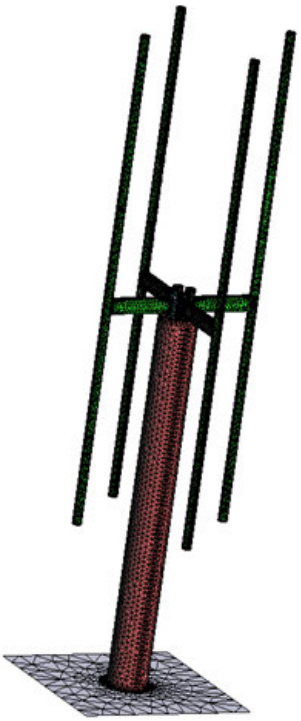

FIGURE 10. Antenna sub-domain (730, 179 tetrahedra, 765, 425 edges).

by applying a process of approximating a desired continuous current distribution by populating the aperture with N discrete antenna elements. An optimization procedure must then be performed to ensure that each radiator has a unique angular coordinate to prevent shadowing. The initial array configuration is the sunflower array, and then, the radii (from the center of the aperture) are modified using the optimization procedure (maintaining the side lobe level almost unchanged while modifying the antenna angular coordinate). The procedure was performed at first with the densified array configuration, but only half of the antennas were used in the GRAVES receiving array. Then, we were provided with the coordinate of the second half of the antennas. The scanning angle area is far from broadside (elevation angle between 45° and 75°) which means that shadowing and coupling effects between the elements that compose the array become stronger by densifying the array. This must be evaluated to qualify the overall performance of the array.

The accurate analysis of this kind of array is not a trivial task. The analysis of the array can involve considering either the periodic and infinite lattice method [39] thanks to periodic boundaries on a unit cell and to a Floquet-Bloch formalism, or by considering the periodic but finite array method [40]. However, an extrapolation to sparse arrays is not possible, since the mutual coupling and shadowing effects generate almost similar radiation patterns, which means that constructive and destructive interferences are visible at almost the same radiation pattern angles for all of the antennas. The interferences will increase the overall gain variation over the scanning area after applying digital beamforming (DBF).

TABLE 1. Computational statistics.

Mesh parameters	
Antenna sub-domain (unknowns)	765, 425
Skeleton interface problem (unknowns)	157.6 millions
Total unknowns of the array	10.47 billions
Simulation parameters	
Number of sub-domains	13, 692
Number of cores (Intel Xeon E5-2680v4)	13, 692
Number of iterations (interface problem)	300
Stopping criterion	$\epsilon = 10^{-2}$
Elapsed time (per antenna)	17 minutes
Memory peak (per core)	3.5 Gb

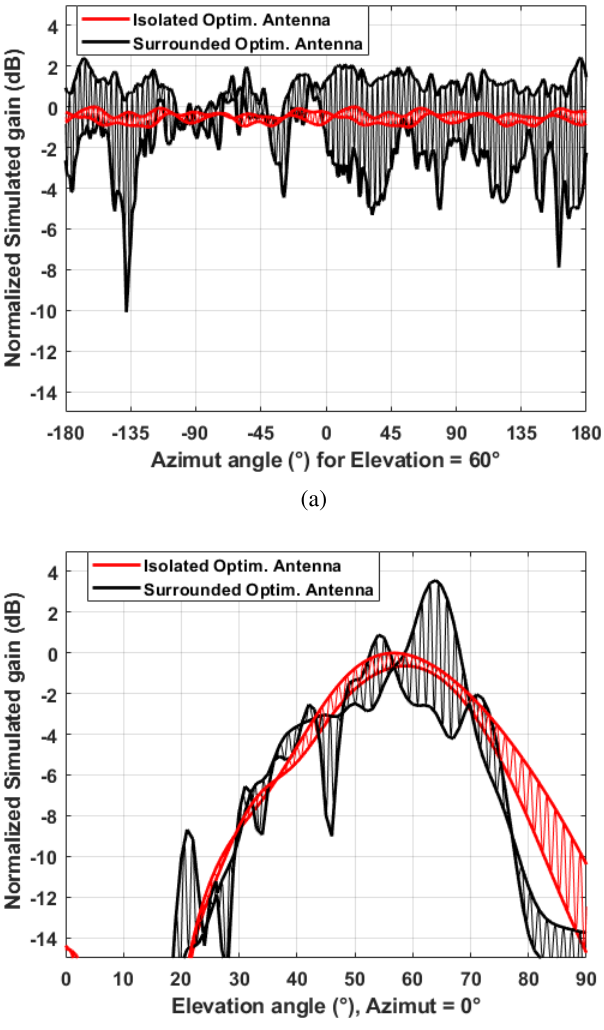

FIGURE 11. Normalized (maximum gain of isolated optimized antenna) radiation pattern in rotating linear polarization of the isolated optimized antenna and one surrounded optimized antenna located in the middle of the densified sparse array along (a) the azimuth angle and (b) the elevation angle.

The interest of using a sparse array configuration where strong coupling and shadowing effects are present is that interferences still apply but at different angles, which means that after applying DBF, the interferences are averaged, which allows a much more stable overall gain over the scanning

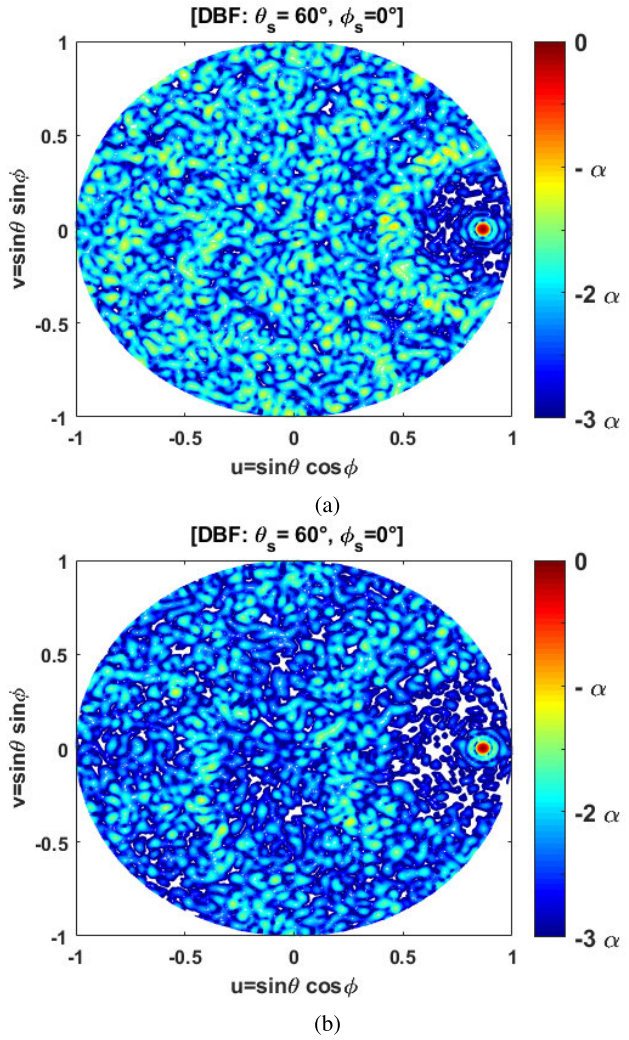

FIGURE 12. Normalized radiation pattern after digital beamforming (with α a fixed value) for a scanning angle of 60° in elevation and 0° in azimuth using (a) the initial array and (b) the densified array.

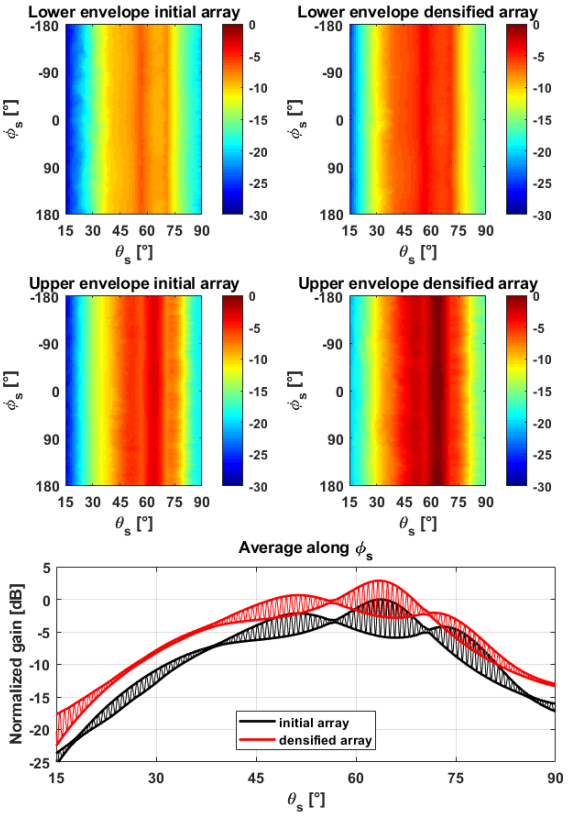

FIGURE 13. Normalized (maximum gain of embedded-element array) gain mapping [upper figures] of the initial and densified sparse arrays considering both the upper and lower envelopes and [lower figure] the normalized gain averaged along the azimuth angles for the initial and densified sparse arrays.

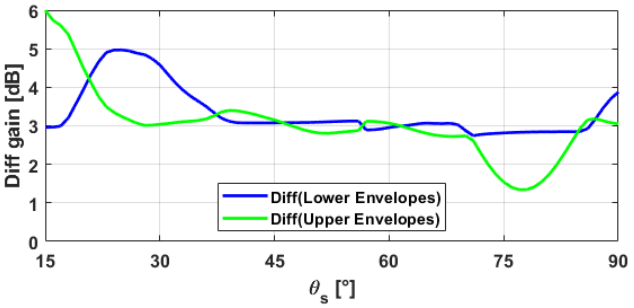

FIGURE 14. Difference in gain between the initial and densified sparse array, considering the upper and lower envelopes.

area. However, a full-wave simulation is required, in order to take into account all of the interactions. As discussed previously, commercial electromagnetism simulation tools such as CST Microwave Studio [13] or HFSS [14] do not allow for the full-wave simulation of the entire sparse array due to the prohibitive number of unknowns of the complete mesh. The chosen strategy is the use of the FACTOPO code developed at ONERA which is based on the Finite Element Method (FEM) coupled with FETI-2LM domain decomposition methods [12], [15]–[17], [31], [41] implemented on parallel machines with thousands of processing cores (clusters HPC).

The general principle for Maxwell equations is to decompose the global computational domain into non-overlapping sub-domains in which local solution fields are calculated by solving the local finite element system with a direct method [42]. Then, an iterative solution of the interface problem is implemented based on a Krylov sub-space method [30]. As explained in paragraph III, the sub-domain decomposition is performed using three types of sub-domains, each of size 0.5×0.5 m^2 to reconstruct the geometry of the complete array. Figure 10 represents the mesh of the antenna sub-domain.

The antenna sub-domain embeds the antenna geometry with surrounding Absorbing Boundary Conditions (ABC) and a Perfect Electrical Conductor (PEC) at the boundary $z = 0$, while the ground plane sub-domain is of the same size but without the antenna geometry. The air sub-domain is an empty sub-domain with ABC boundary conditions. Figure 3 shows the sub-domain decomposition considering the densified sparse array. A total of 13, 692 sub-domains

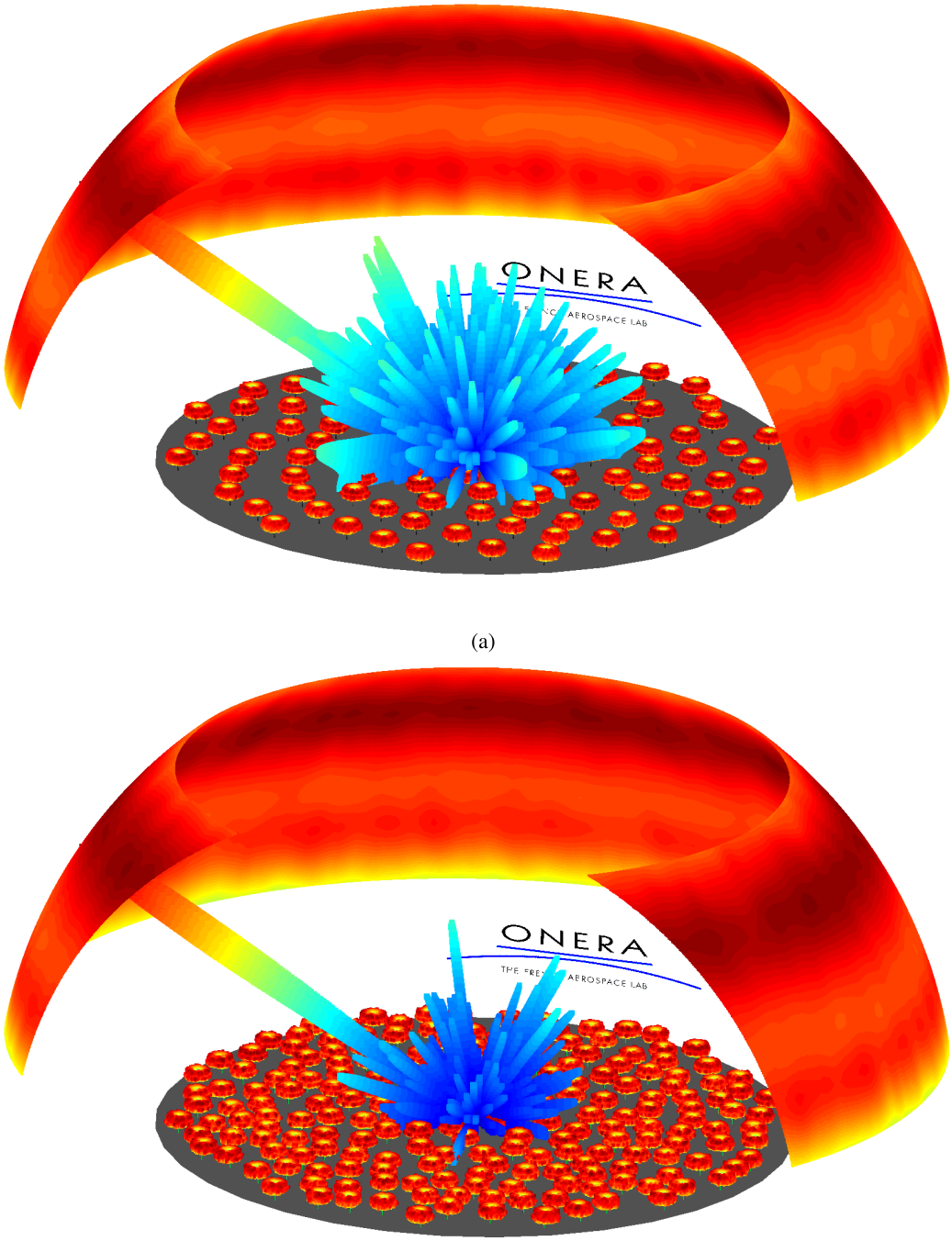

FIGURE 15. (a) Overall initial sparse array configuration with the embedded normalized radiation patterns, the normalized radiation pattern after digital beamforming, and the overall normalized gain mapping; (b) Overall densified sparse array configuration with the embedded radiation patterns, the normalized radiation pattern after digital beamforming, and the overall normalized gain mapping.

are used, considering thoses corresponding to antennas, air sub-domains and ground sub-domains. This simulation requires 13, 692 processing cores, each handling one sub-domain. We used ONERA's NEC scalar parallel supercomputer SATOR, which has 620 computing nodes, with 28 Intel Xeon Broadwell E5-2680v4 processing cores each, for a total of 17, 360 processing cores. 4 GB of memory is allocated for each core. Hence, the antenna-sub-domain needs to be accurately meshed to be handled with 4 GB of memory.

The computation statistics are given in Tab.1. The total number of unknowns in the 3D sparse array computational domain is 10.47 billion and the number of unknowns on the

skeleton interface is 157.6 million. The interface problem was solved through 300 iterations in 17 minutes per antenna with a stopping criteria of 10^{-2}. During this simulation campaign of the initial and densified sparse arrays, a total of 277 hours on 13, 692 processing cores corresponding to 3.8 millions cumulated hours was necessary.

Figure 11 shows a comparison between the radiation pattern of the isolated optimized antenna and the radiation pattern of one surrounded optimized antenna located in the middle of the densified sparse array. This shows that strong coupling and shadow effects are present, with a gain variation of about 12 dB for the same elevation angle between the lower and upper envelopes.

By using the surrounded complex radiation patterns of the initial and densified arrays, DBF is applied for a given scanning angle set (elevation angle θ_s, azimuth angle ϕ_s) and the maximum gain of this set is extracted as shown in Figure 12. As an illustration, a stable improvement of 2.5 dB of the Normalized Integrated Side Lobe Ratio (NISLR) by densifying the sparse array by a factor of 2 is obtained by DDM full-wave simulation. The NISLR improvement provides the ability to detect weaker targets in the neighborhood of bright targets. The DBF is performed for all sets to provide a gain mapping after DBF over the full scanning area.

In Figure 13 the gain mapping is shown for both the initial and the densified sparse array configuration, considering the lower and upper envelopes. After averaging the gain mapping along the azimuth axis, in the bottom plot of Figure 13 the gain variation of each configuration using the rotating linear polarization is shown.

By comparing the upper and the lower envelopes of the configurations, Figure 14 makes it possible to demonstrate that, even with strong shadow and coupling effects due to a densification of the sparse array by a factor of two, we obtain an increase in gain of approximately 3 dB in the required FoV for an elevation angle between 15° and 70°. Figure 15 shows the normalized 3D radiation patterns of all of the elements (lower envelope), the digital beamforming in one direction and the gain mapping for the initial and densified sparse array configurations respectively.

VI. CONCLUSION

A new methodology efficiently handling the simulation of large sparse arrays in the VHF band through FETI-2LM domain decomposition method is proposed in this work. An efficient implementation of a meshing strategy that consists in generating the sparse array by populating a regular periodic grid is proposed, and a block Krylov recycling method is implemented to accelerate the simulation of the hundreds of embedded antenna diagrams of the GRAVES sparse array. These novelties implemented in the FETI-2LM allowed the performance of the GRAVES radar sparse receiving array densification be investigated. The results were obtained using a full-wave simulation, thanks to the capability of ONERA's FACTOPO code combined with the use of the NEC scalar parallel supercomputer SATOR to simulate such configuration with an enormous number of unknowns (10.47 billion unknowns). Those intensive simulations, which required 3.8 million cumulated hours and the use of 13, 692 Intel Xeon Broadwell E5-2680v4 computing cores, have made it possible to take into account all of the phenomena, in order to ensure that this densification will not affect the overall performances and to demonstrate the positive impact on the overall link budget while improving the ability to detect weaker targets in the neighborhood of bright targets. The foreseen evolutions will make GRAVES an even more valuable key contributor to the SST segment.

ACKNOWLEDGMENT

Multi-source FETI simulation algorithms for non periodic applications have been optimized in part thanks to the Grand Equipement National de Calcul Scientifique through the Grant c2014109083.

REFERENCES

[1] T. Michal, J. Eglizeaud, and J. Bouchard, "Graves: The new French system for space surveillance," in *Proc. 4th Eur. Conf. Space Debris*, vol. 587, 2005, p. 61.
[2] T. Donath, T. Schildknecht, P. Brousse, J. Laycock, T. Michal, and P. Ameline, "Proposal for a European space surveillance system," in *Proc. 4th Eur. Conf. Space Debris*, vol. 587, 2005, p. 31.
[3] T. Castaings, B. Pannetier, F. Müller, and M. Rombaut, "Track initiation in low-earth-orbit objects using statistical modeling of sparse observations," *IEEE Trans. Aerosp. Electron. Syst.*, vol. 51, no. 1, pp. 258–269, Jan. 2015.
[4] T. Castaings, B. Pannetier, F. Müller, and M. Rombaut, "Sparse data association for low earth orbit tracking," in *Proc. IEEE Aerosp. Conf.*, Mar. 2012, pp. 1–7.
[5] *Air Force Space Surveillance System*. Accessed: Aug. 26, 2018. [Online]. Available: https://en.wikipedia.org/wiki/AirForceSpaceSurveillance System
[6] *Eglin AFB Site C-6*. Accessed: Aug. 27, 2019. [Online]. Available: https://en.wikipedia.org/wiki/EglinAFBSiteC-6
[7] *Space Fence*. Accessed: Jun. 15, 2019. [Online]. Available: https://en.wikipedia.org/wiki/SpaceFence
[8] *Ballistic Missile Early Warning System*. Accessed: Dec. 12, 2018. [Online]. Available: https://fr.wikipedia.org/wiki/BallisticMissileEarlyWarning System
[9] *Radar Voronezh*. Accessed: May 8, 2019. [Online]. Available: https://fr.wikipedia.org/wiki/BallisticMissileEarlyWarningSystem
[10] J.-M. Jin, *The Finite Element Method in Electromagnetics*, 2nd ed. New York, NY, USA: Wiley, 2002.
[11] J. L. Volakis, A. Chatterjee, and L. C. Kempel, *Finite Element Method for Electromagnetics, Antennas, Circuits Microwaves and Scattering Applications* (The IEEE: OUP Series on Electromagnetic Wave Theory), D. G. Dudley, Ed. 1998.
[12] A. Barka, "Integration of antennas onboard vehicles and diffraction by large and complex structures with multiple-domain–multiple-methods techniques," *Proc. IEEE*, vol. 101, no. 2, pp. 280–297, Feb. 2013.
[13] *CST Microwave Studio*. Accessed: Sep. 2019. [Online]. Available: https://www.3ds.com/products-services/simulia/products/cst-studio-suite/
[14] *ANSYS HFSS*. Accessed: Sep. 2019. [Online]. Available: https://www.ansys.com/products/electronics/ansys-hfss
[15] A. Barka, P. Soudais, and D. Volpert, "Scattering from 3-D cavities with a plug and play numerical scheme combining IE, PDE, and modal techniques," *IEEE Trans. Antennas Propag.*, vol. 48, no. 5, pp. 704–712, May 2000.
[16] A. Barka and P. Caudrillier, "Domain decomposition method based on generalized scattering matrix for installed performance of antennas on aircraft," *IEEE Trans. Antennas Propag.*, vol. 55, no. 6, pp. 1833–1842, Jun. 2007.
[17] A. Barka and C. Picard, "Implementation of spectral basis functions in BEM/FEM/GSM domain decomposition methods devoted to scattering and radiation applications," *Comput. Phys. Commun.*, vol. 178, pp. 438–448, Mar. 2008.

[18] R. Chiniard, A. Barka, and O. Pascal, "Hybrid FEM/floquet modes/PO technique for multi-incidence RCS prediction of array antennas," *IEEE Trans. Antennas Propag.*, vol. 56, no. 6, pp. 1679–1686, Jun. 2008.

[19] A. Barka and N. Douchin, "Asymptotic simplifications for hybrid BEM/GO/PO/PTD techniques based on a generalized scattering matrix approach," *Comput. Phys. Commun.*, vol. 183, pp. 1928–1936, Sep. 2012.

[20] P. Bjørstad and O. B. Widlund, "Iterative methods for the solution of elliptic problems on regions partitioned into substructures," *SIAM J. Numer. Anal.*, vol. 23, no. 6, pp. 1097–1120, 1986.

[21] C. Farhat and F.-X. Roux, "A method of finite element tearing and interconnecting and its parallel solution algorithm," *Int. J. Numer. Methods Eng.*, vol. 32, no. 6, pp. 1205–1227, Oct. 1991.

[22] A. de La Bourdonnaye, C. Farhat, A. Macedo, F. Magoulès, and F. Roux, "A non-overlapping domain decomposition method for the exterior Helmoltz problem," *Contemp. Math.*, vol. 218, pp. 42–66, Jan. 1998.

[23] G. Cohen, L. Halpern, and P. Joly, *Mathematical and Numerical Aspects of Wave Propagation Phenomena*. Philadelphia, PA, USA: SIAM, 1991, pp. 44–52.

[24] C. Farhat, L. Crivelli, and F. X. Roux, "Extending substructure based iterative solvers to multiple load and repeated analyses," *Compt. Methods Appl. Mech. Eng.*, vol. 117, pp. 195–209, Jul. 1994.

[25] R. Tezaur, A. Macedo, and C. Farhat, "Iterative solution of large-scale acoustic scattering problems with multiple right hand-sides by a domain decomposition method with Lagrange multipliers," *Int. J. Numer. Methods Eng.*, vol. 51, pp. 1175–1193, Aug. 2001.

[26] M. N. Vouvakis, Z. Cendes, and J.-F. Lee, "A FEM domain decomposition method for photonic and electromagnetic band gap structures," *IEEE Trans. Antennas Propag.*, vol. 54, no. 2, pp. 721–733, Feb. 2006.

[27] K. Zhao, V. Rawat, S.-C. Lee, and J.-F. Lee, "A domain decomposition method with nonconformal meshes for finite periodic and semi-periodic structures," *IEEE Trans. Antennas Propag.*, vol. 55, no. 9, pp. 2559–2570, Sep. 2007.

[28] M. L. Parks, E. de Sturler, G. Mackey, D. D. Johnson, and S. Maiti, "Recycling Krylov subspaces for sequences of linear systems," *SIAM J. Sci. Comput.*, vol. 28, no. 5, pp. 1651–1674, Oct. 2006.

[29] Z. Peng, M. B. Stephanson, and J.-F. Lee, "Fast computation of angular responses of large-scale three-dimensional electromagnetic wave scattering," *IEEE Trans. Antennas Propag.*, vol. 58, no. 9, pp. 3004–3012, Sep. 2010.

[30] F.-X. Roux and A. Barka, "Block Krylov recycling algorithms for FETI-2LM applied to 3-D electromagnetic wave scattering and radiation," *IEEE Trans. Antennas Propag.*, vol. 65, no. 4, pp. 1886–1895, Apr. 2017.

[31] A. Barka, S. Matos, J. R. Costa, and C. A. Fernandes, "Assessment of FETI DDM methodologies for the simulation of high gain Ka-band transmit arrays," in *Proc. Int. Symp. Antennas Propag. (ISAP)*, Oct./Nov. 2017, pp. 1–2.

[32] *METIS—Serial Graph Partitioning and Fill-Reducing Matrix Ordering*. Accessed: Sep. 2019. [Online]. Available: http://glaros.dtc.umn.edu/gkhome/views/metis

[33] M. F. Xue and J. M. Jin, "A hybrid conformal/nonconformal domain decomposition method for multi-region electromagnetic modeling," *IEEE Trans. Antennas Propag.*, vol. 62, no. 4, pp. 2009–2021, Apr. 2014.

[34] *Gid the Personal Pre and Post Processor*. [Online]. Available: https://www.gidhome.com

[35] F.-X. Roux and A. Barka, "FETI methods," in *Computational Electromagnetics: Recent Advances and Engineering Applications*, R. Mittra, Ed. New York, NY, USA: Springer, 2014.

[36] J. C. Nedelec, "Mixed finite elements in $\mathbb{R}^3$," *Numer. Math.*, vol. 35, no. 3, pp. 315–341, Sep. 1980.

[37] Y. Saad, *Iterative Methods for Sparse Linear Systems*. Philadelphia, PA, USA: SIAM, 2003. [Online]. Available: https://www-users.cs.umn.edu/~saad/books.html

[38] A. Ramalli and P. Tortoli, "256-element density-tapered spiral matrices for ultrasound phased imaging," in *Proc. Ultrason. Symp. (IUS)*, Sep. 2014, pp. 2087–2090.

[39] R. J. Mailloux, *Phased Array Antenna Handbook*. Norwood, MA, USA: Artech House, 2017.

[40] B. Lesur, A. Maati, M. Thevenot, C. Menudier, E. Arnaud, T. Monediere, C. Melle, D. Chaimbault, and A. Karas, "A large antenna array for Ka-band satcom-on-the-move applications—Accurate modeling and experimental characterization," *IEEE Trans. Antennas Propag.*, vol. 66, no. 9, pp. 4586–4595, Sep. 2018.

[41] F.-X. Roux and A. Barka, "Block krylov recycling algorithms for FETI-2LM applied to 3-D electromagnetic wave scattering and radiation," *IEEE Trans. Antennas Propag.*, vol. 65, no. 4, pp. 1886–1895, Apr. 2017.

[42] *Intel MKL PARDISO, Developer Reference for Intel Math Kernel Library—Fortran*. Accessed: May 23, 2019. [Online]. Available: https://software.intel.com/en-us/mkl-developer-reference-fortran-intel-mkl-pardiso-parallel-direct-sparse-solver-interface

ANTOINE JOUADÉ received the M.Sc. degree in signal processing and telecommunication engineering from the University of Rennes 1, Rennes, France, and the Ph.D. degree in signal processing and telecommunications from the Institute of Electronics and Telecommunications, University of Rennes 1, in 2017. He was an Intern with the Antenna and Sub-Millimeter Section, European Space and Technology Center, European Space Agency, ESA ESTEC, Noordwijk, The Netherlands. He is currently a Research Engineer with the French Aerospace Laboratory (ONERA), Electromagnetism and Radar Department. His research interests include radar, signal processing, and associated antennas.

ANDRÉ BARKA received the M.Sc. and Ph.D. degrees in applied mathematics from the University of Bordeaux, France, in 1986 and 1990, respectively, and the Habilitation à Diriger des Recherches (HDR) degree from the University of Toulouse, in 2008. He is currently a Ph.D. Advisor with the GEET Doctoral School, Toulouse. He joined ONERA, in 1989, where he is in charge of developing advanced multidomain and multimethod techniques combining integral equations, finite element methods, and asymptotic techniques. He was the Work-Package Manager of advanced modeling activities in the FP6 IPAS European Project and the H2020 EPICEA European/Canadian Project. From September 2016 to September 2017, he was an Invited Researcher with the Telecommunications Institute, University of Lisbon, Portugal, through a research convention with ONERA, the French DoD, and the University of Lisbon. He is also a Senior Scientist with more than 20 years of research experience in computational electromagnetics (and especially in domain decomposition methods), in various application fields, such as electromagnetic compatibility, radar cross section, and antennas. His current research interests include the design and realization of new antenna concepts based on metamaterials, and advanced domain decomposition methods, including finite element tearing and interconnecting (FETI) and integral equation domain decomposition methods (IE-DDM). He has been a member of the Board of *Computer Physics Communications* journal, since 2006, and a Computational Electromagnetic Specialist Editor.